ORIGINAL ARTICLE

Relationship between tissue characteristics and mechanical properties of coronary plaques: a comparison between integrated backscatter intravascular ultrasound (IVUS) and speckle-tracking IVUS

Shinichiro Tanaka[1] · Masanori Kawasaki[2] · Toshiyuki Noda[3] · Tomonori Segawa[1] · Makoto Iwama[3] · Hiroto Yagasaki[3] · Takahiro Ueno[3] · Takashi Yoshizane[3] · Takashi Kato[3] · Takahiro Fuseya[1] · Sachiro Watanabe[3] · Taro Minagawa[4] · Shinya Minatoguchi[5] · Hiroyuki Okura[6]

Abstract

High-risk coronary plaques have certain morphological characteristics. Thus, comprehensive assessment is needed for the risk stratification of plaques in patients with coronary artery disease. Integrated backscatter intravascular ultrasound (IB-IVUS) has been used successfully used to evaluate the tissue characteristics of coronary plaques; however, the mechanical properties of plaques have been rarely assessed. Therefore, we developed Speckle-tracking IVUS (ST-IVUS) to evaluate the mechanical properties of coronary plaque. This study aimed to evaluate the relation between the tissue characteristics of coronary plaques using IB-IVUS and their mechanical properties using ST-IVUS. We evaluated 95 non-targeted plaques in 95 patients undergoing elective percutaneous coronary intervention to the left anterior descending artery. We set regions of interest (ROIs) in the cross-sectional images of coronary plaques where we divided 120 degree plaques into four quadrants (every 30 degrees), with the center at the area of maximum atheroma thickness. We measured relative calcification area (%CA, relative fibrous area (%FI) and relative lipid pool area (%LP) in a total of 380 ROIs. In ST-IVUS analysis, we measured strain in the circumferential direction of the lumen area (LA strain: %), the external elastic membrane area strain (EEM strain: %), and strain in the radial direction (radial strain: %). On global cross-sectional area IB-IVUS analysis, the %CA was $1.2 \pm 1.2\%$; the %FI was $49.0 \pm 15.9\%$, and the %LP was $49.7 \pm 16.5\%$. In ST-IVUS analysis, the LA strain was $0.67 \pm 0.43\%$; the EEM strain was $0.49 \pm 0.33\%$, and the radial strain was $2.02 \pm 1.66\%$. On regional analysis, the %LP was not associated with the LA strain ($r = -0.002$ $p = 0.97$), the EEM strain ($r = -0.05$ $p = 0.35$), or with the radial strain ($r = -0.04$ $p = 0.45$). These trends were seen between the %FI and the LA strain ($r = 0.02$ $p = 0.74$), the %FI and the EEM strain ($r = 0.05$ $p = 0.35$), and the %FI and the radial strain ($r = 0.04$ $p = 0.50$). A significant correlation was only observed between the %CA and the LA strain ($r = -0.15$ $p = 0.0038$). Our findings indicate that the associations between mechanical properties and tissue characteristics lacked statistical significance, more often than not, and that it is necessary to evaluate the mechanical properties as well as plaque characteristics for risk stratification of coronary plaques.

Keywords Coronary artery disease · Tissue characteristics · Integrated backscatter IVUS · Mechanical properties · Speckle-tracking IVUS

Introduction

Acute coronary syndrome is a life-threatening condition [1, 2] that is commonly caused by the rupture of vulnerable plaques. Plaque rupture has been frequently associated with certain morphological features such as high lipid content in the coronary plaque, or inflammation of the fibrous cap [3–6]. Another cause is thrombi forming on top of plaques without their rupture (plaque erosion). Erosion most often occurs on areas of pathological intimal thickening or fibroatheromas. Calcified nodules are a rare cause of coronary thrombosis [3]. Thus, comprehensive assessment is needed for the risk stratification of high-risk plaques in patients with coronary artery disease. Intravascular ultrasound (IVUS) has played an important role in the assessment

✉ Shinichiro Tanaka
 shin19711015@yahoo.co.jp

Extended author information available on the last page of the article

and identification of rupture-prone coronary plaques, and integrated backscatter (IB)-IVUS is one of the most useful methods for the pathological assessment of coronary plaques. Previous research has shown that IB-IVUS had high sensitivity and specificity (90–95%) for the tissue characterization of coronary plaques compared to histology as the gold standard method [4, 7–12]. Hence, we developed speckle-tracking (ST)-IVUS as a technique that allows the assessment of the mechanical properties of plaques by pulsatile intramural pressure during a cardiac cycle [13, 14]. Although atherosclerotic changes consist of both structural (atherosis) and functional (sclerosis) components [12], the relationship between the mechanical and compositional properties of coronary atherosclerosis has rarely been assessed [15, 16]. Thus, we explored the potential relationship between the compositional properties (determined by IB-IVUS) and mechanical properties (determined by ST-IVUS) of coronary plaques in matched cross-sectional areas in patients with stable coronary heart disease.

Materials and methods

This retrospective study was conducted in accordance with the principles of the Declaration of Helsinki and the Ethical Guidelines for Medical and Health Research Involving Human Subjects by the Ministry of Health, Labor, and Welfare and Ministry of Education, Culture, Sports, Science, and Technology of Japan. It was approved by the Ethics Committee of Gifu Prefectural General Medical Center (approval number: 137). Informed consent was obtained in the form of opt-out on the Gifu Prefectural General Medical Center's website for the study.
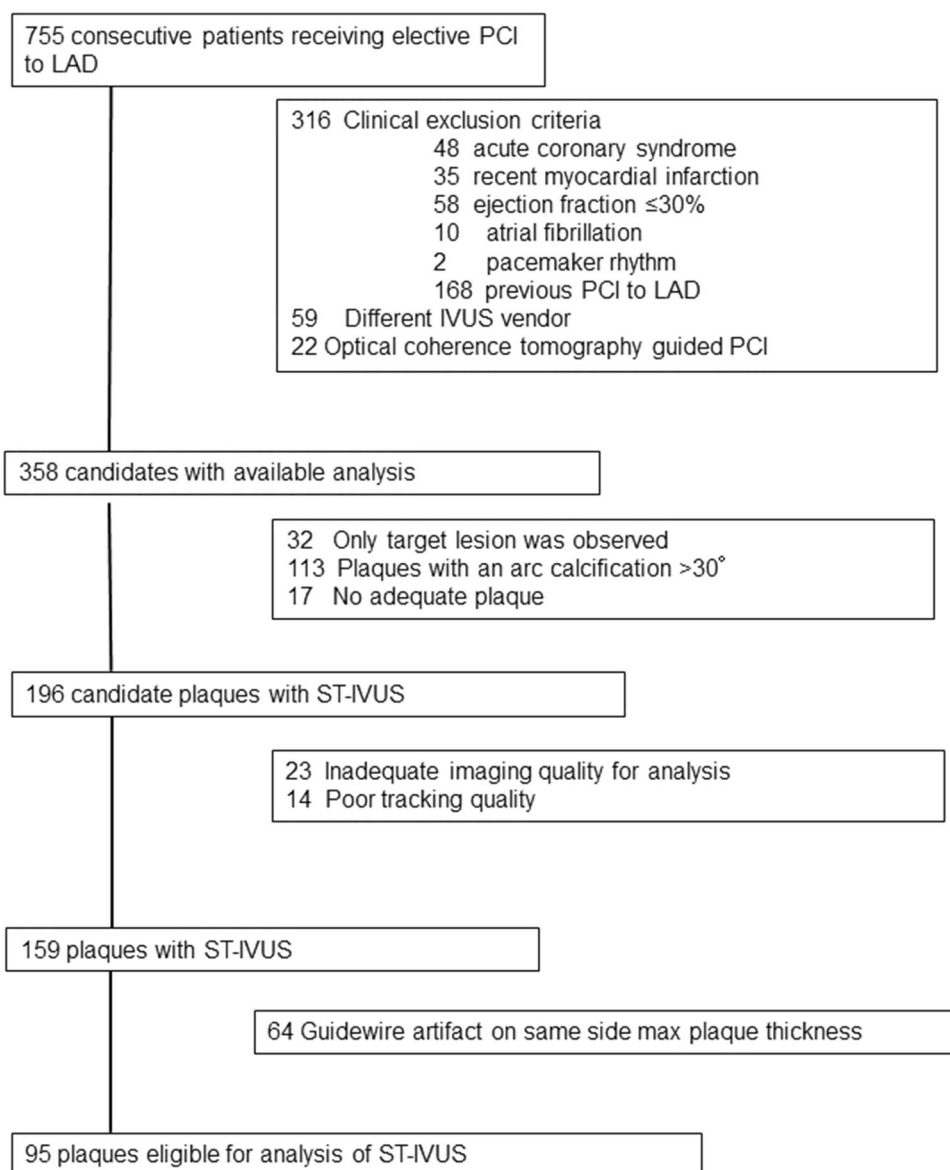
Study design and eligibility

We enrolled 755 consecutive patients with stable angina pectoris who underwent elective percutaneous coronary interventions (PCIs) to the left anterior descending arteries (LAD). We included only the left anterior descending arteries, because right coronary and left circumflex arteries often had ectasia and are not typically sites of coronary atherosclerotic lesions [7, 12]. We excluded patients who had unstable angina or myocardial infarction within the previous 3 months, an ejection fraction ≤ 30%, atrial fibrillation, or frequent ventricular premature beats. Patients with low systolic pressure (≤ 100 mmHg) during catheterization were also excluded. Additionally, patients who previously underwent PCI in the LAD were excluded because the treated lesions were thought to show different behaviors resulting from the medial replacement of smooth muscle cells with hyalinized collagen after PCI [7, 12]. To avoid errors in the mechanical and compositional analysis of the regional plaque, we also excluded plaques where the artifact caused by the guidewire existed on the same side of maximum atheroma thickness. Non-targeted plaques located proximal to the site of the PCI target lesions were evaluated, since there was a pressure difference of by 5 mmHg between proximal and distal pressures, even in atheromatous coronary arteries without clinically significant stenosis [12, 17]. After enrolling eligible patients, plaques with arc calcification > 60° were also excluded in the analysis. A total of 95 plaques in 95 patients fulfilled the eligibility criteria. The details of study population are summarized in Fig. 1.

The coronary risk factors were as follows: hypertension, defined as patients with documented hypertension; hyperlipidemia, defined as patients with documented hyperlipidemia; diabetes mellitus (DM), defined as being previously diagnosed with DM, intake of any anti-hyperglycemic medication, or a HbA1c level > 6.5%; smoking, defined as smoking at baseline, or having quit smoking < 1 year before the study; chronic kidney disease (CKD), defined as an estimated glomerular filtration rate (eGFR) of < 60 mL/min/1.73 m^2.

IVUS procedure, conventional IVUS analysis, IB-IVUS and data acquirement

During each index PCI procedure, a 38-MHz mechanically rotating IVUS catheter (ViewIT, Terumo Corporation, Tokyo, Japan) was inserted distally as far as possible into the vessel. Continuous monitoring via ultrasound imaging was performed while withdrawing the catheter through the artery segment at a constant rate of 0.5 mm/s. Electrocardiographic (ECG) data were continuously displayed on conventional IVUS images. The values for systemic pressure were obtained from the tip of the guiding catheter in the ostium of the left main coronary trunk and were continuously displayed on the monitor. IVUS data were stored on a hard disk for offline analysis. Using IVUS analysis (VISIATLAS Ver. 2, Terumo Corporation, Tokyo, Japan), luminal cross-sectional area (LA), external elastic membrane (EEM) cross-sectional area (CSA), plaque area (PA; PA = EEM CSA − LA), and % plaque area (PA/EEM × 100) were quantified from cross-sectional images. This analysis was performed at the onset of the QRS complex (end-diastole) and the termination of the T-wave (end-systole). The position and axis of the IVUS catheter might have slightly changed during the cardiac cycle with the automated pull-back IVUS system. Therefore, we adopted the average of the IVUS measurements taken in three cardiac cycles (one cardiac cycle proximal, and distal to the site of minimal lumen diameter from the onset of the first QRS complex to the fourth QRS complex) as a standard measurement of plaque mechanical behavior. That is, the averages were four cross-sectional areas at end-diastole and three cross-sectional areas at end-systole. The thickness of the analyzed lesion

Fig. 1 Flowchart of the study
population

```
┌─────────────────────────────────────────────────┐
│ 755 consecutive patients receiving elective PCI  │
│ to LAD                                            │
└─────────────────────────────────────────────────┘
                    │
                    │   ┌────────────────────────────────────────────┐
                    │   │ 316  Clinical exclusion criteria            │
                    │   │        48  acute coronary syndrome          │
                    │   │        35  recent myocardial infarction     │
                    │   │        58  ejection fraction ≤30%           │
                    │   │        10  atrial fibrillation              │
                    │   │        2   pacemaker rhythm                 │
                    │   │        168 previous PCI to LAD              │
                    │   │ 59    Different IVUS vendor                 │
                    │   │ 22 Optical coherence tomography guided PCI  │
                    │   └────────────────────────────────────────────┘
                    │
┌─────────────────────────────────────────────────┐
│ 358 candidates with available analysis           │
└─────────────────────────────────────────────────┘
                    │
                    │   ┌────────────────────────────────────────────┐
                    │   │ 32   Only target lesion was observed        │
                    │   │ 113  Plaques with an arc calcification >30° │
                    │   │ 17   No adequate plaque                     │
                    │   └────────────────────────────────────────────┘
                    │
┌─────────────────────────────────────────────────┐
│ 196 candidate plaques with ST-IVUS               │
└─────────────────────────────────────────────────┘
                    │
                    │   ┌────────────────────────────────────────────┐
                    │   │ 23  Inadequate imaging quality for analysis │
                    │   │ 14  Poor tracking quality                   │
                    │   └────────────────────────────────────────────┘
                    │
┌─────────────────────────────────────────────────┐
│ 159 plaques with ST-IVUS                         │
└─────────────────────────────────────────────────┘
                    │
                    │   ┌──────────────────────────────────────────────────┐
                    │   │ 64 Guidewire artifact on same side max plaque     │
                    │   │    thickness                                      │
                    │   └──────────────────────────────────────────────────┘
                    │
┌─────────────────────────────────────────────────┐
│ 95 plaques eligible for analysis of ST-IVUS      │
└─────────────────────────────────────────────────┘
```

depended on heart rate and pullback speed (0.5 mm/s). With a heart rate of 60 beat/min the analysis length is 0.5 mm.

Integrated backscatter was evaluated as previously described [7, 10–12]. Briefly, ultrasound backscattered signals were acquired using a 38 MHz rotating IVUS catheter; the signals were digitized and subjected to spectral analysis. Using a fast Fourier transform, integrated backscatter (IB) values for each tissue characteristics were calculated as an average power of the frequency component of the backscattered signal from a small volume of tissue and measured in decibels. The representative color-coded maps of the cross-sectional coronary artery plaques were constructed using IB cut-off points for discriminating calcification, fibrosis, and lipid pools, as described previously [7, 10–12]. We averaged relative lipid pool area (%LP), relative fibrous area (%FI), and relative calcified area (%CA) in seven cross-sections.

The eccentricity rate was calculated at the lesion as follows: (maximum plaque plus media thickness − minimum plaque plus media thickness)/maximum plaque plus media thickness. The remodeling index was defined as the ratio of the EEM area at the lesion of MLA to the EEM area at the proximal reference site. There were reports on the localization of tissue characteristics [7] and stress localization of plaques [18, 19]. Accordingly, we set regions of interest (ROIs) at plaques of 120°, with their centers at the area of maximum atheroma thickness and subdivided each region of interest (ROI) into the following four 30° quadrants: inner clockwise (inner-clockwise), inner counterclockwise (inner-counter), lateral clock wise (lateral-clockwise), and lateral counterclockwise (lateral-counter). The max atheroma thickness was automatically measured by IVUS analysis system. On the other hand, the angle at which the ROI was determined

was based on the center of IVUS catheters as a landmark. The ROIs were partitioned according to the closest part to max atheroma thickness (Fig. 2).

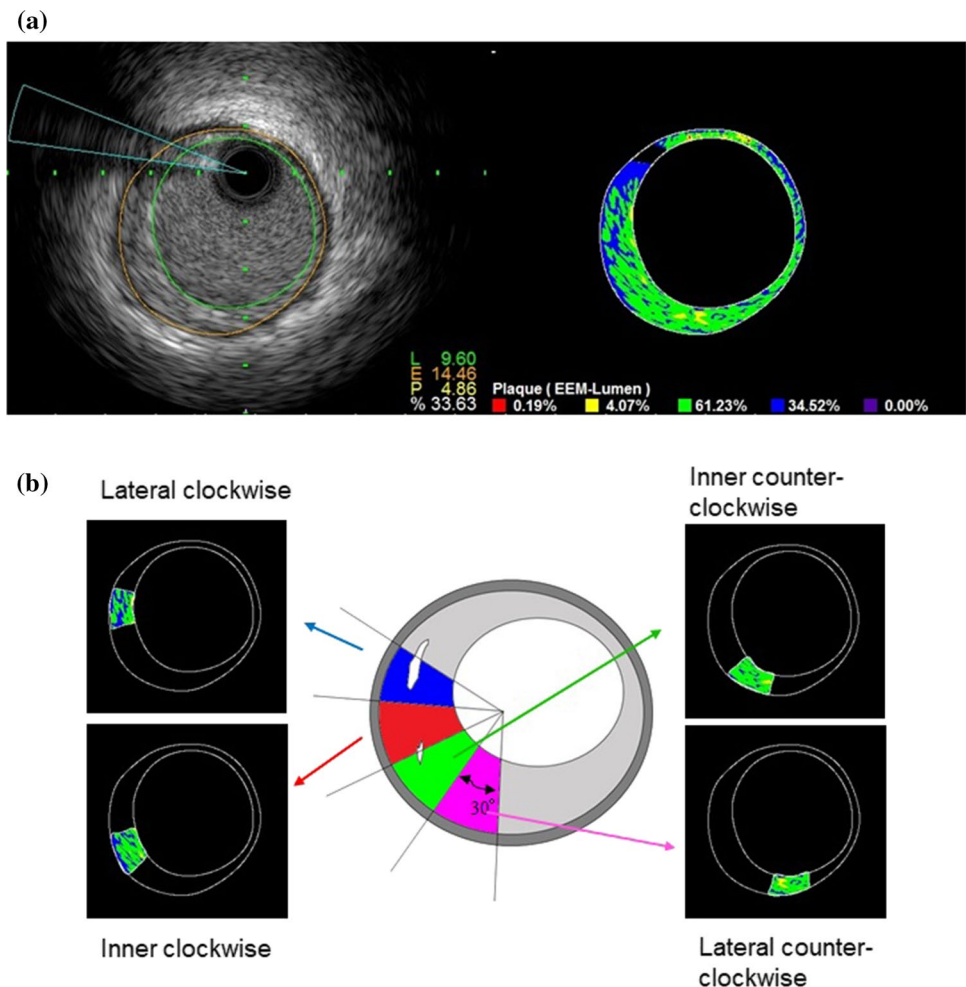## Speckle-tracking intravascular ultrasound (ST-IVUS)

The ST-IVUS system adopted velocity vector imaging (VVI) software (Syngo Velocity Vector imaging, Siemens). IVUS data were limited to the thickness of the analyzed lesion matched by frame numbers and were set to the ST-IVUS system offline. Manual placement of a lumen border and EEM over one frame is then automatically tracked throughout the cardiac cycle. The software allows editing of the initial trace if tracking was poor. The operator could repeat the imaging and readjust or change the tracing. We could measure the strain in every 7.5° along the lumen contour captured during the cardiac cycle. Strains of the adjoined sample-speckles were calculated in radial or circumferential direction. Strain (%) represented the ratio between the distance at the voluntary phase and the distance at the QRS complex phase in circumferential and radial directions. We defined strain (%) as the width of the strain curve in a cardiac cycle. We measured the strain of the lumen area in a circumferential direction (LA strain: %), the strain of the external elastic membrane area in a circumferential direction (EEM strain: %), and the strain in a radial direction (radial strain: %). Because strains were affected by blood pressure, we corrected strain with a logarithm of the pulse pressure at the time of measurement [20]; corrected strain = strain (%)/ ln (pulse pressure). As aforementioned, the four quadrants of the ROIs (two clockwise and two counter-clockwise from the area of maximum atheroma thickness) were selected in cross-sectional area (at every 30° from the center of the vessel), and the strain was measured as an average of each 7.5° within the ROIs (Fig. 3).

Validation, reliability, and reproducibility of strain by ST-IUVS

Using 20 cross-sectional images from 20 patients, we set crescent-shaped calcified lesions located in coronary plaques (that were suitable for observation) as ROIs to ensure validation, reliability and reproducibility. The position and axis of the IVUS slightly changed during the

Fig. 2 Representative image of integrated backscatter intravascular ultrasound (IB-IVUS). **a** Conventional IVUS image and IB-IVUS image for global cross sectional analysis. **b** For regional analysis, region of interest (ROI) was divided into four clusters of plaque centered at the area of maximum atheroma thickness. Each ROI was defined as inner clockwise (inner-clockwise), inner counterclockwise (inner-counter), lateral clock wise (lateral-clockwise), and lateral counterclockwise (lateral-counter)

Fig. 3 Representative image of speckle-tracking intravascular ultrasound (ST-IVUS). **a** LA strain is shown. The speckle in every 7.5° were captured along the lumen contour, and the 48 sample speeds were measured during three cardiac cycles automatically. We described an average curve and measured global strain. **b** LA strain of region of interest (ROI) strain was also measured by the same method. *LA strain* the strain of the lumen area in a circumferential direction, *EEM strain* the strain of the external elastic membrane area in a circumferential direction, *radial strain* the strain in a radial direction
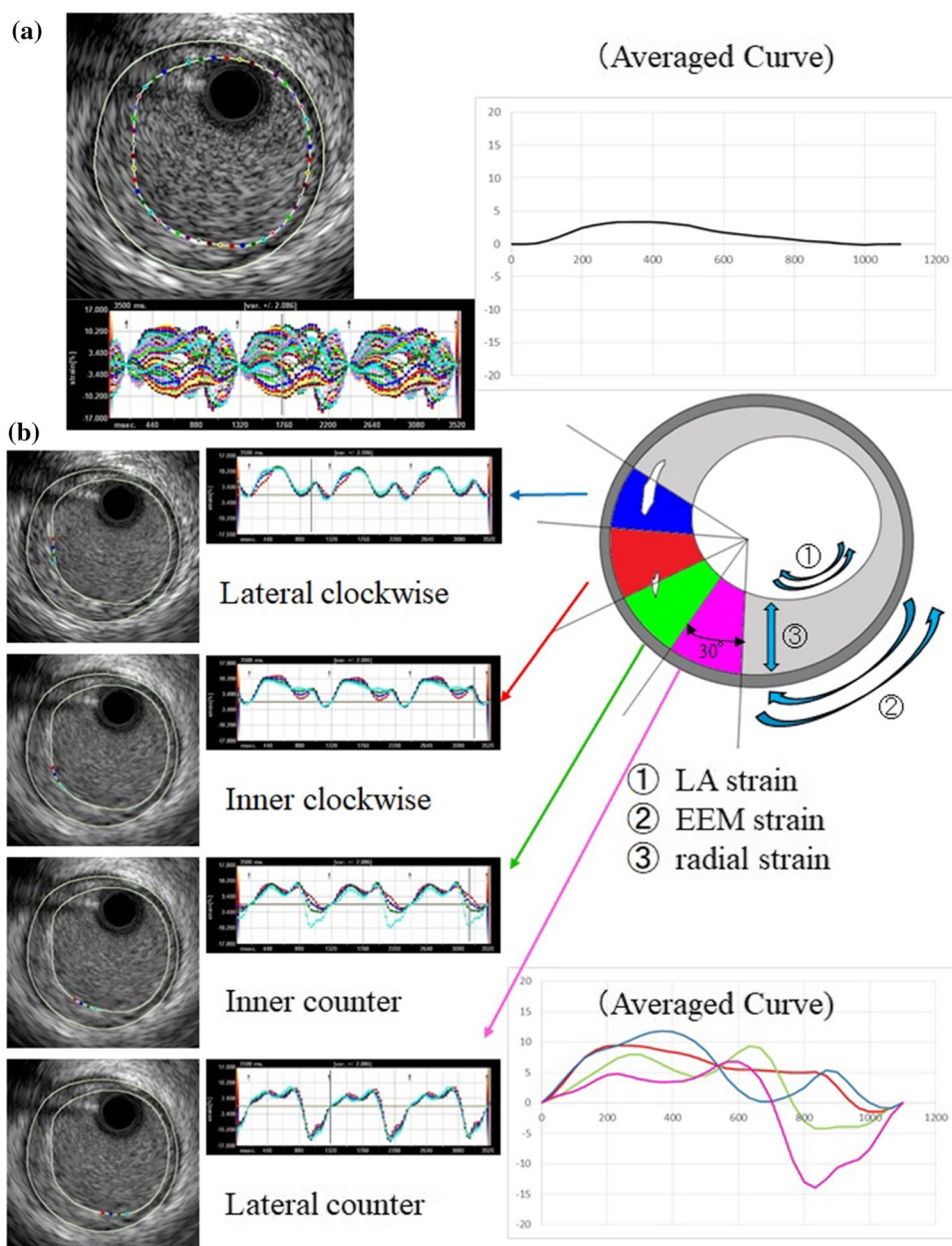
cardiac cycle leading to change of the ROIs as well. Three points were selected at both ends and near the apex of the crescent-shaped calcification for speckle tracking by ST-IVUS. The average value of the strain at these three points was obtained. This allowed the observers to easily confirm the tracking visually. If tracking was inadequate, the ROI could be re-tracked. The strain values of the ROI obtained from the ST-IVUS (ST-calc) were compared to the rate of change of the length of the ROI obtained by the manual method (ST-Manu). Intra-and inter-observer variabilities were also applied in accordance with the above (Fig. 4).

Furthermore, we determined intra- and inter-observer variability of LA strain, EEM strain, and radial strain without corrected pulse pressure in 20 randomly selected of cross-sectional area.

We determined the intra-observer variability twice by one observer at 7-day intervals. The inter-observer variability was determined by two observers in a blinded manner.

Statistical analysis

Continuous data are expressed as means ± standard deviation or as proportions. Pearson's correlation coefficient analysis and simple regression analysis were used for continuous data. Categorical data were expressed as frequencies and percentages. For comparison among the ROI

(a)

ST-manu; 0.034%

ST-manu; 3.2 %

(b)
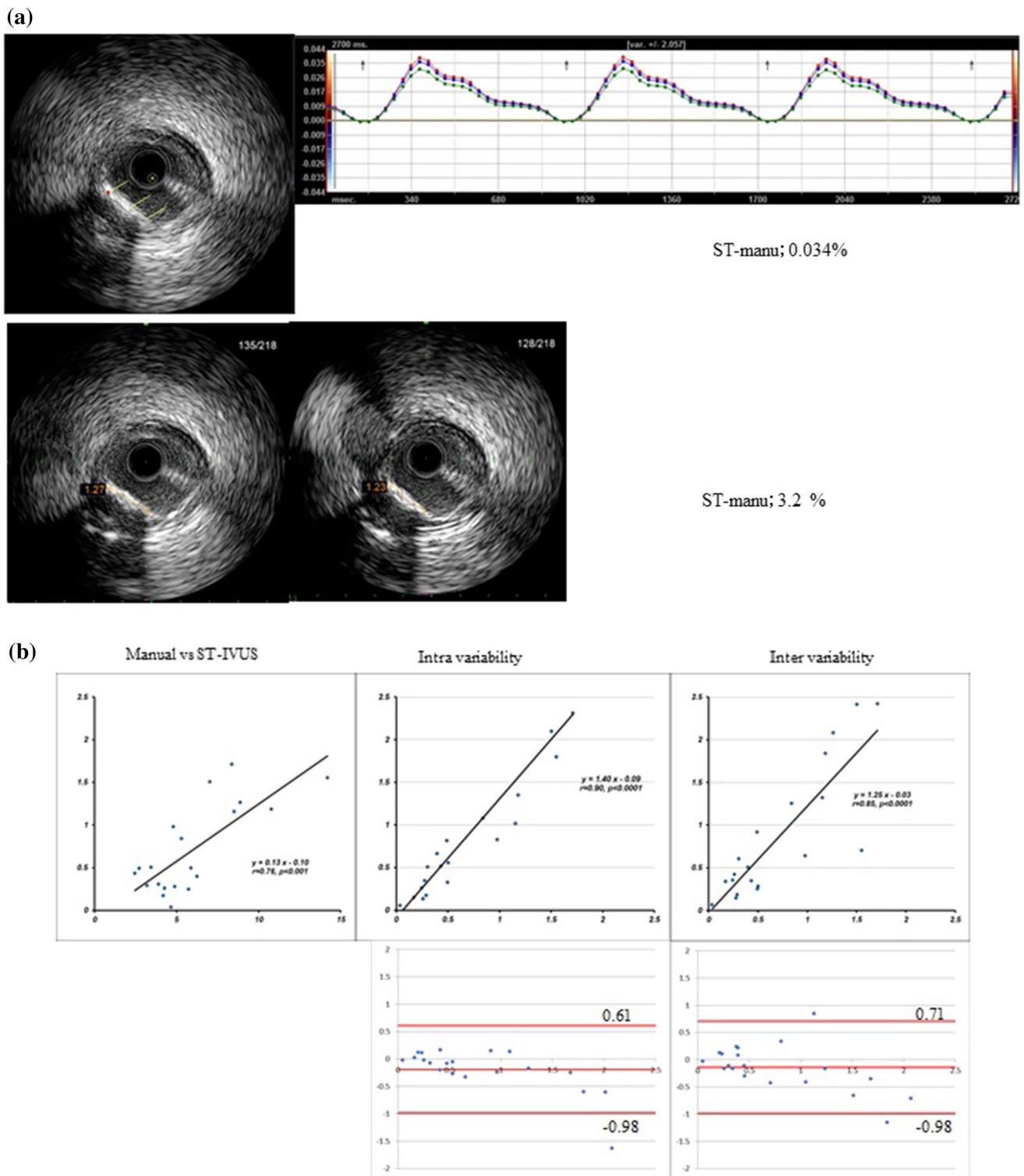
Fig. 4 Validation, reliability and reproducibility of strain by speckle-tracking intravascular ultrasound (ST-IVUS). A crescent-shaped calcified lesion suitable for observation located in the coronary plaque was set as a region of interest (ROI) for validation, reliability and reproducibility. **a** The strain values of the ROI obtained from the ST-IVUS (ST-calc) were compared to the rate of change of the length of the ROI obtained by the manual method (ST-Manu); **b** Comparison of the strain value of the ST-calc, ST-Manu, and Bland–Altman analysis of ST-manu of intra- and inter-observer variability

groups, ANOVA was used. When ANOVA was significant, Tukey–Kramer test was used as a post hoc test. Statistical significance was set at $p < 0.05$. All analyses were performed using Microsoft Excel ver. 2019 and SAS software version 5.0 (SAS Institute Inc., Cary, NC, USA).

Results

Validation, reliability, and reproducibility of strain by ST-IUVS

The ST-calc was $0.71 \pm 0.52\%$, while the ST-Manu was $6.0 \pm 2.9\%$. The intra-observer correlation coefficient and variability in the ST-calc were 0.90 and $-0.19 \pm 0.41\%$, respectively. The inter-observer correlation coefficient and variability were 0.85 and $-0.14 \pm 0.43\%$, respectively. There was a significant correlation between the strain value measured by the ST-calc and the ST-Manu. The ST-calc (y) was approximately 13% of the ST-Mau (x) indicated by IB-IVUS ($y = 0.13x-0.10$, $r = 0.76$, $p < 0.001$) at the same cross-section (Fig. 4).

The intra-observer correlation coefficient and relative differences in LA strain, EEM strain, and radial strain without corrected pulse pressure were 0.90 and $-0.24 \pm 1.69\%$, 0.97 and $0.04 \pm 0.28\%$, and 0.86 and $-1.57 \pm 3.77\%$, respectively. The inter-observer correlation coefficient and relative differences in LA strain, EEM strain, and radial strain without corrected pulse pressure were 0.93 and $0.82 \pm 1.10\%$, 0.96 and $-0.02 \pm 0.41\%$, and 0.82 and $-0.06 \pm 3.91\%$, respectively.

Characteristics and background of the patients

The clinical backgrounds of the 95 study participants are shown in Table 1. The mean age was 69.3 years. Seventy-three patients (76.8%) had hypertension; 61 patients (64.2%) had hyperlipidemia; 46 patients (48.4%) had diabetes; 28 patients smoked; 42 patients had CKD and two patients received hemodialysis. Twenty-four patients (28.8%) had a history of myocardial infarction, and 38 (40.0%) had undergone coronary revascularization; all these patients received percutaneous coronary interventions (PCI) to right coronary artery and/or left circumflex artery. There were none who had received coronary artery bypass grafting previously in this study. At the time of the IVUS study, the systolic blood pressure was 145.8 ± 27.7 mmHg; the diastolic blood pressure was 68.5 ± 13.2 mmHg, and the heart rate was 72.5 ± 13.4 /min. One patient had a history of aspirin allergy and received P2Y12 inhibitors alone. In addition, 1 patient developed liver damage after receiving P2Y12 inhibitors and had substituted them with two doses of aspirin. Statins were administered to 55.8% of participants, and low-density lipoprotein (LDL)-cholesterol levels were 107.2 ± 35.9 mg/

Table 1 Patient characteristics

	Total	%
Numbers of cases	95	
Age (years)	69.3 ± 9.2	
Male	74	77.9
Hypertension	73	76.8
Hyperlipidemia	61	64.2
Diabetes mellitus	46	48.4
Smoker	28	29.5
CKD	42	44.2
Hemodialysis	2	2.1
Prior myocardial infarction	24	25.3
Previous revascularization	38	40.0
Left circumflex	12	12.6
Right	19	20.0
Right and left circumflex	6	6.3
Ejection fraction (%)	65.0 ± 7.68	
Blood pressure (mmHg)		
Systolic	145.8 ± 27.7	
Diastolic	68.5 ± 13.2	
Heart rate (/min)	72.5 ± 13.4	
Total cholesterol (mg/dl)	189.5 ± 40.3	
Triglycerides (mg/dl)	160.5 ± 60.3	
HDL-cholesterol (mg/dl)	51.3 ± 15.8	
LDL-cholesterol (mg/dl)	107.2 ± 35.9	
HbA1C ()	6.2 ± 0.9	
Creatinine (mg/dl)	0.97 ± 0.61	
eGFR (ml/min/1.73 m^2)	63.8 ± 20.7	
C-reactive protein (mg/dl)	0.24 ± 0.55	
Medication		
Aspirin	94	98.9
P2Y12 inhibitors	94	98.9
ARB/ACE	58	61.1
Statin	53	55.8
β-Blocker	32	33.7
Ca-blocker	45	47.4
Nitrates/nicorandil	45	47.4
Diuretics	9	9.5
Ezetimibe	2	2.1
Insulin	6	6.3
Biguanide	12	12.6
DPP-4	22	23.2
Sulfonylurea	13	13.7

Blood pressure and heart rate were taken at the time of the IVUS study

CKD chronic kidney disease (eGFR < 60 ml/min/1.73 m^2), *HDL* high density lipoprotein, *LDL* low density lipoprotein, *eGFR* estimated glomelular filtration rate, *ARB* angiotensin II receptor blocker, *ACE* angiotensin converting enzyme inhibitor, *DPP-4* dipeptidyl peptidase-4 inhibitor

dl. The HbA1c level was $6.2 \pm 0.9\%$ under diet, exercise, and anti-hyperglycemic medication.

Global cross-sectional area analyses

Conventional IVUS parameters, parameters of tissue characteristics by IB-IVUS, and strains derived from ST-IVUS are shown in Table 2. The %plaque area was $49.3 \pm 9.1\%$ (range 32.5–70.8%). On IB-IVUS analysis, the %CA was 1.2 ± 1.2; the %FI was 49.0 ± 15.9, and the %LP was

Table 2 Intravascular ultrasound (IVUS) observation

Numbers of patients	95
Quantitative analysis	
LA (mm^2)	7.40 ± 2.02
EEM (mm^2)	14.7 ± 3.3
Plaque area (mm^2)	7.27 ± 2.25
% Plaque area (%)	49.3 ± 9.1
Remodeling Index	1.00 ± 0.04
Eccentricity rate	0.87 ± 0.04
IB-IVUS measurement (%)	
Calcification (%)	1.2 ± 1.2
Fibrosis (%)	49.0 ± 15.9
Lipid pool (%)	49.7 ± 16.5
ST-IVUS measurement	
LA strain (%)	2.85 ± 1.74
EEM strain (%)	2.09 ± 1.38
Radial strain (%)	8.52 ± 6.88
Pressure corrected	
LA strain (%)	0.67 ± 0.43
EEM strain (%)	0.49 ± 0.33
Radial strain (%)	2.02 ± 1.66

IB-IVUS integrated backscatter IVUS, *ST-IVUS* speckle-tracking IVUS, *LA strain* the strain of the lumen area in a circumferential direction, *EEM strain* the strain of the external elastic membrane area in a circumferential direction, *radial strain* the strain in a radial direction

$49.7 \pm 16.5\%$. Regarding measurement by ST-IVUS, after adjusted pulse pressure, the LA strain was $0.67 \pm 0.43\%$; the EEM strain was $0.49 \pm 0.33\%$, and the radial strain was $2.02 \pm 1.66\%$. Relations among conventional IVUS measurements, IB-IVUS measurements, and ST-IVUS measurements are shown in Table 3. There were significant relations between the % plaque area and the radial strain ($r = -0.33$, $p = 0.001$), and between the %CA and the LA strain ($r = -0.21$, $p = 0.049$). There were no significant relations among other parameters.

Relation between tissue characterization and mechanical properties on regional analyses

The plaque area, and the parameters derived from the IB-IVUS and ST-IVUS of every ROI are shown in Table 4. Average plaque areas of the inner-clockwise, the inner-counter, the lateral-clockwise, and the lateral-counter were 1.15 ± 0.35 mm^2, 1.13 ± 0.33 mm^2, 0.91 ± 0.29 mm^2, and 0.92 ± 0.31 mm^2, respectively. The plaque areas near the area of plaque maximum thickness (the inner-clockwise and the inner-counter) were larger than those of the ROIs far from the area of plaque maximum thickness (the lateral-clockwise and the lateral-counter). In the EEM strain, a significant difference was observed in post hoc test after ANOVA for the lateral-counter site ($2.60 \pm 2.08\%$) and the inner-clockwise site ($1.93 \pm 1.66\%$). However, there were no significant differences in the tissue characteristics and the mechanical properties among the other ROIs. Relations between the tissue characteristics derived from IB-IVUS and the strains derived from ST-IVUS are shown in Table 5. In the entire ROIs, there were significant associations between the EEM strain and the plaque area of the ROI, and between the LA strain and the %CA (Table 5 and Fig. 5). Regarding the relationship among the main plaque components (the %FI, the %LP) and the strain, significant relationships were found only between the EEM strain and the %FI and between the EEM strain and the %LP at the inner-clockwise site.

Table 3 Correlation between strains corrected pulse pressure and tissue component in global cross-sectional area

	LA strain (%)		EEM strain (%)		Radial strain (%)	
	r	*p*	*r*	*p*	*r*	*p*
% plaque area	0.05	0.61	-0.24	0.020	-0.33	0.001
plaque area (mm^2)	0.18	0.091	-0.13	0.23	-0.20	0.053
Remodeling index	0.02	0.84	0.09	0.42	0.05	0.61
Eccentricity rate	0.01	0.94	0.17	0.095	0.19	0.07
Calcification (%)	-0.21	0.049	-0.06	0.55	-0.18	0.080
Fibrosis (%)	-0.09	0.40	0.20	0.053	-0.10	0.35
Lipid pool (%)	0.10	0.35	-0.19	0.067	0.11	0.29

All strains were corrected by pulse pressure

LA strain the strain of the lumen area in a circumferential direction, *EEM strain* the strain of the external elastic membrane area in a circumferential direction, *radial strain* the strain in a radial direction

Table 4 Parameters of IB-IVUS and ST-IVUS in each region of interest (ROI)

|	Lateral-counter	Inner-counter	Inner-clockwise	Lateral-clockwise	p (ANOVA)
Plaque (ROI) area (mm^2)	0.92 ± 0.31	1.13 ± 0.33	1.15 ± 0.35	0.91 ± 0.29	< 0.0001
IB-IVUS					
Calcification (%)	1.3 ± 1.9	1.3 ± 1.9	1.3 ± 1.9	1.0 ± 1.5	0.55
Fibrosis (%)	50.2 ± 18.7	48.8 ± 18.0	48.0 ± 19.0	47.0 ± 19.1	0.69
Lipid pool (%)	48.5 ± 19.3	50.0 ± 18.4	50.8 ± 19.2	52.2 ± 19.5	0.61
ST-IVUS					
LA strain (%)	2.18 ± 1.42	2.15 ± 1.36	2.11 ± 1.36	2.44 ± 1.60	0.40
EEM strain (%)	2.60 ± 2.08*	2.07 ± 1.55	1.93 ± 1.66*	2.03 ± 1.43	0.034
Radial strain (%)	10.74 ± 7.65	10.16 ± 7.84	9.44 ± 6.91	9.24 ± 5.25	0.41

All strains were corrected by pulse pressure

LA strain the strain of the lumen area in a circumferential direction, *EEM strain* the strain of the external elastic membrane area in a circumferential direction, *radial strain* the strain in a radial direction

*$p < 0.05$ post hoc test (Turkey–Kramer)

Table 5 Correlation between ST-IVUS observation corrected pressure and tissue component in each region of interest (ROI)

	plaque area (mm^2)		Calcification (%)		Fibrosis (%)		Lipid pool (%)	
	r	p	r	p	r	p	r	p
Total								
LA strain (%)	− 0.01	0.88	− 0.15	0.0038	0.02	0.74	− 0.002	0.97
EEM strain (%)	− 0.18	0.0004	0.01	0.90	0.05	0.35	− 0.05	0.35
Radial strain (%)	− 0.02	0.70	0.04	0.49	0.04	0.50	− 0.04	0.45
Lateral-counter								
LA strain (%)	− 0.11	0.29	− 0.20	0.052	− 0.09	0.40	0.11	0.32
EEM strain (%)	− 0.17	0.10	0.001	0.99	− 0.18	0.09	0.17	0.10
Radial strain (%)	− 0.10	0.32	0.13	0.2	0.07	0.54	− 0.08	0.47
Inner-counter								
LA strain (%)	− 0.01	0.91	− 0.18	0.09	0.15	0.15	− 0.13	0.23
EEM strain (%)	− 0.18	0.086	− 0.06	0.59	0.15	0.15	− 0.14	0.18
Radial strain (%)	0.04	0.73	0.09	0.41	0.13	0.21	− 0.14	0.19
Inner-clockwise								
LA strain (%)	0.12	0.23	− 0.11	0.29	0.14	0.19	− 0.13	0.24
EEM strain (%)	− 0.17	0.091	0.10	0.33	0.21	0.05	− 0.22	0.039
Radial strain (%)	0.06	0.55	− 0.12	0.25	− 0.08	0.47	0.09	0.41
Lateral-clockwise								
LA strain (%)	0.04	0.74	− 0.09	0.42	− 0.09	0.42	0.09	0.39
EEM strain (%)	− 0.12	0.25	− 0.06	0.55	0.05	0.61	− 0.05	0.64
Radial strain (%)	0.11	0.3	− 0.02	0.83	− 0.03	0.8	0.02	0.85

All strains were corrected by pulse pressure

LA strain the strain of the lumen area in a circumferential direction, *EEM strain* the strain of the external elastic membrane area in a circumferential direction, *radial strain* the strain in a radial direction

Discussion

In this study, we evaluated the relations between the tissue characteristics derived from IB-IVUS and the strains derived from ST-IVUS. The principal findings are as follows: in the global cross-sectional area analyses, the tissue characteristics of coronary plaques (the %FI and the %LP) had no associated strains; a significant (albeit weak) correlation was observed between %CA and the strain. And even performing regional analyses, the relationship among the strain and the main components (the %FI and the %LP) were weakly associated in a partial set of the ROIs.
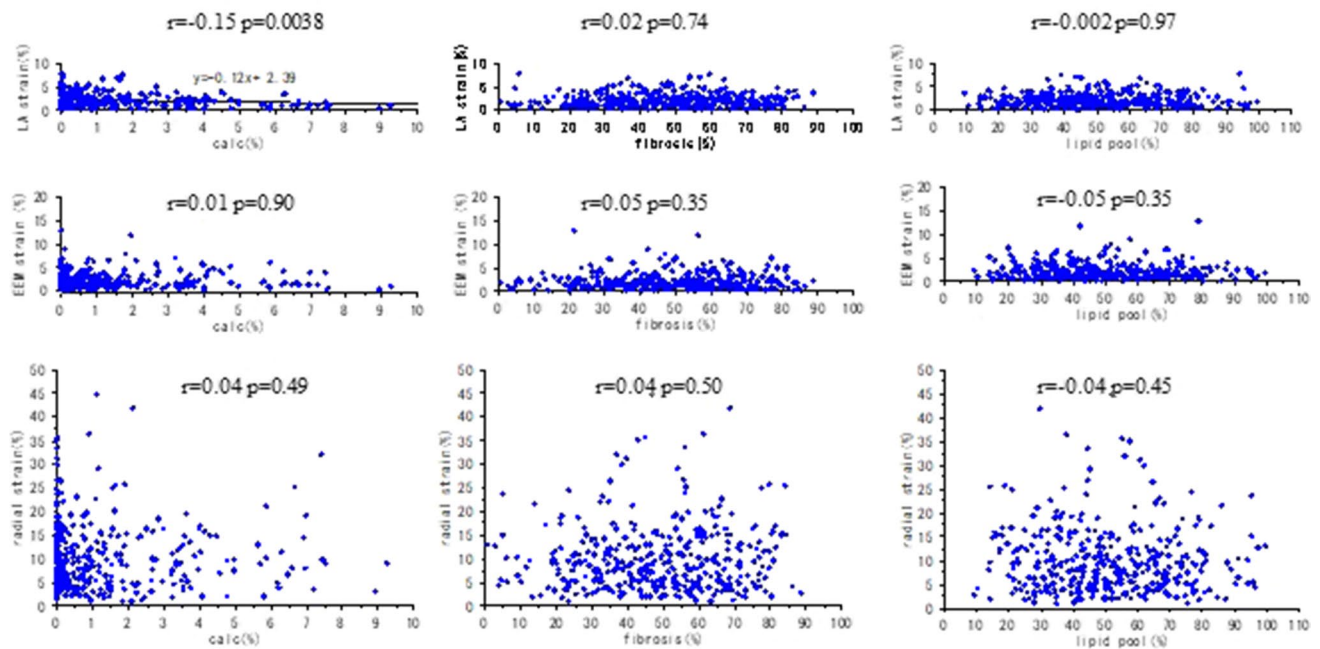
Fig. 5 Relation between tissue characteristics and mechanical properties on regional analysis. All strains were corrected by pulse pressure

Similarly, in a previous study using virtual histology IVUS (VH-IVUS) and palpography, a significant inverse relationship was observed between relative calcium area and strain level [15]. We expected to find a low strain value in a hard component such as calcification. Furthermore, in the present study, the main coronary tissue characteristics (lipid pool, fibrous component) were not associated with strains. This result also corresponded to a previous study where the relations among strains derived from palpography and tissue characteristics derived from VH-IVUS were not significant (strains vs. %fibrosis; $r = 0.06$, $p = 0.55$, strains vs. %fibrolipidemic $r = -0.13$, $p = 0.15$) [15]. This trend was also observed in the Rotterdam classification score categorized by maximum strain value [16]. In a carotid artery study, which compared strain derived carotid artery ultrasonography to histology from carotid endarterectomy, no significant correlation was found between strain parameters and cap thickness, smooth muscle cell concentration, or macrophage concentration [21]. The study pointed out that strain is not a direct result of the presence of one histological component, but a representation of the interaction among all components. Our findings support that in clinical practice, strain does not directly reflect the presence of a single plaque component in coronary plaques.

From investigation of the relationship between tissue characteristics by IB-IVUS and plaque compliance from manual area measurements during the cardiac cycle, there was no significant correlation between lumen compliance and the relative lipid pool volume, whereas EEM compliance was significantly correlated with the relative lipid pool volume [12]. In our study, in addition to the association among the EEM strain and the variables related to plaque amount (the %plaque area and the plaque area) or among the radial strain and those, which is considered to be influenced by blood pressure, there were non-significant but trends in the association among the EEM strain and the main components (the %FI and the %LP) or among the radial strain and those. Furthermore, this relationship was weak but a significant for the inner-clockwise ROI. The possible reasons why there were the ROIs where mechanical properties and tissue characteristics were unrelated and the ROIs where they are related were that the interaction among all components mentioned above [21], and that there would be strain within each ROI that were affected by adjacent ROIs and plaque opposite sites, such that a certain amount of deformation was shared by the lipid pool plaque on the opposite side of the ROI. On the other hand, the LA strain and the main plaque components were poorly related. These results may imply that lumen changes during the cardiac cycle may be related to endothelial function, independent of EEM changes and plaque components [12, 22]. Pressure-inducing mechanical stress has an influence on endothelial function [23, 24]. Circumferential strain measured by carotid ultrasonography with 2-dimensional speckle tracking seems to be superior to methods assessing functional endothelial dysfunction [25]. Our results indicate that the LA strain was not associated with the main components of coronary plaques. A previous

study on arteries with mild stenosis (no significant stenosis) demonstrated that coronary endothelial dysfunction is associated with the presence of a necrotic core as assessed by VH-IVUS [26] or a lipid core plaque by near infrared spectroscopy [27]. These results seem to be contrary to our findings. However, another study reported that epicardial endothelial dysfunction was associated with optical coherence tomography-identified macrophages and microchannels in mild coronary atherosclerosis, and found no association between endothelial function and OCT-identified lipid-rich plaques [28]. Additionally, Keymel et al. showed that flow-mediated dilation of brachial arteries as a maker for endothelial function and fractional diameter changes as a maker for mechanical properties of external diameter of the artery independently represented the endothelial function and vascular structure of brachial arteries [22]. These discrepancies may result from differences in the stages of atherosclerosis in the involved patients; since our study population required revascularization, endothelial function seemed to be already impaired. Further studies are needed to assess the relation between the LA circumferential strain and endothelial function.

Palpography was already validated in an ex-vivo model to identify thin-capped fibroatheromas [29, 30]. However, in previous substudy, the strain values were found to be no different between plaques with a thin or a thick fibrous cap, as evaluated by IVUS [16]. Furthermore, derived strain value does not provide any additional diagnostic information with respect to the VH-IVUS and does not specifically identify plaques at a higher risk of events [16]. The radio frequency data can only reflect the displacement along the ultrasound beam. This strain image of palpography is a radial strain map limited to the direction of the ultrasound beam. ST-IUVS can evaluate the strain in the coronary conduit in circumferential and radial directions. However, the speckle-tracking method remains comparatively reproductive because of such as sample-interchange during a cardiac cycle or imaging qualities [31]. Nevertheless, mechanical properties of coronary plaques play an important role in plaque rupture, and strain measurement may potentially identify rupture-prone plaques. Previous coronary atherosclerosis models showed that mechanical stress increased in the side opposite to the maximum plaque thickness if there was no typical lipid pool in the coronary plaque apart from the rupture-prone plaque [18]. This previous study showed that the regions of maximum circumferential stress lie where there is a difference in the fibrous cap over the lipid pool or on the luminal wall near the thinnest plaque section [18]. Additionally, considering that in our study there was a weak but significant difference between the lateral-counter site and the inner-clockwise site with respect to the EEM strain, we should also approach not only strain value, but also "where" spot is higher strain in the future.

A vulnerable plaque is also caused by mechanical fatigue of the plaque caused by exposure to pressure and repeated cycles of distension and elastic recoil of the arterial wall [25]. Whether mechanical fatigue generated by reduced strain exposes the plaque to a greater risk of rupture than mechanical fatigue generated by greater strain remains to be determined. Further studies would be necessary using ST-IVUS.

In conclusion, we investigated the association between tissue characteristics and mechanical properties using IB-IVUS and ST-IVUS. In this present study, although there were weak significant associations between some aspects of the mechanical properties and the tissue characteristics, more often than not, the associations lacked statistical significance in plaques in patients with stable coronary heart disease who required revascularization. For the risk stratification of high risk plaques, it is important to evaluate mechanical properties as well as tissue characteristics.

Clinical implications

Our study findings have important clinical implications. It is well-known that plaque rupture is associated with morphological features such as a large lipid content in coronary plaques or inflammation of the fibrous cap [3, 4]. Pulsatile and repetitive dynamic stress on coronary plaques could also be an alternative index for the risk of rupture [12]. Similar to previous studies [15, 16], our results showed that there was a lack of association between tissue characteristics and mechanical properties in clinical setting during PCI. Because IB-IVUS and ST-IVUS use the same data, information could be obtained by the same pull-back images. Thus, the assessment of coronary mechanical properties and tissue characteristics during PCI may provide us with useful information regarding the risk stratification of patients with coronary heart disease.

Study limitations

This study has several important limitations. Transthoracic echocardiography speckle tracking software operates optimally for strain analysis when the heart is in the same position, not moving during the cardiac cycle. In echocardiography, the heart may be in the same position on the assumption that only a few seconds are requested of the patient at one phase of respiration [31], and speckle tracking software ensures that segments are tracked appropriately. In our study, the position and axis of the IVUS might have slightly changed during the cardiac cycle and IVUS auto-pullback. To overcome this, we performed an average analysis of three cardiac cycles. This might allow us to achieve optimal analysis while using the ST-IVUS system because of the averaged thickness of the analyzed lesion.

Additionally, we analyzed only the proximal left anterior descending arteries, and excluded the right coronary and left circumflex arteries because they often have ectasia that results from medial replacement of smooth muscle cells with hyalinized collagen, which is not typical of coronary atherosclerotic lesions [7, 12].

In this study, although the IB-IVUS system could exclude the area with an artifact due to the guidewire, we included this area in the global CSA analysis from the ST-IVUS images. Therefore, the guidewire artifact might cause errors of the strain value, although the ST-IVUS software made an approximate calculation of the value from sample speckles. However, we obtained similar results in our regional analysis with absolute exclusion of wire artifacts. Although, there was no error of different frames between IB-IVUS and ST-IVUS, we cannot deny that there could be a possibility of a slight gap difference in the setting of ROIs on IB-IVUS and ST-IVUS. Furthermore, the maximum atheroma thickness was automatically measured and determined by the IVUS analysis system, but the angle at which the ROIs were determined was based on the center of the IVUS catheter as a landmark. Although the ROIs were partitioned at the closest part closest to max atheroma thickness, there would be a slight gap because the ROI was determined using the center of IVUS catheters as a landmark. This could be a limitation. Although these were intrinsic errors, they did not arise in the global CSA analysis. However, since we obtained similar results in global CSA analysis and regional analysis, we believe that the setting of ROIs in this study was performed precisely and appropriately.

Moreover, the validation of regional strain in coronary arteries was a weakness in our validation study. This is because the ST-Manu calculated the measurement from the distance between both ends of the calcified lesion, whereas the ST-calc calculated the measurement from the calcified lesion itself. There remained concerns that strain values by ST-IVUS were insufficiently validated, including phantom studies. The previous in-vitro [33] and in-vivo validation studies [34–36] may lead speckle tracking system in this study to permit the accurate assessment of coronary plaque behavior. This is because many speckle-tracking techniques were based on similar principles of detecting and tracking specific patterns in images. While some speckle-tracking imaging software has been properly investigated, the models used to mimic in vitro motion were generally simple [14, 37]. An in-vivo animal validation study also showed that strain was acquired accurately by ultrasonically measuring between two pairs of 2-mm diameter crystals inserted 1–1.5 cm apart using a sonomicrometer in the left ventricle of dogs [36]. Although there was an apparent difference, the speckle tracking method was based on an image-base and was expected to provide similar accuracy. Nevertheless, ST-IVUS was only validated in this study by tracking

calcification during the cardiac cycle, which was insufficient for validation, and further validation studies were needed.

Another limitation was that we did not follow-up patients in our study. We performed IVUS at only one point in time, so unknown or unmeasurable factors could potentially alter the responses at other points in time. A temporary increase in emotional or physical stress triggers an acute event [3], which might affect the dynamic stress of the coronary plaque. Although, we corrected mechanical properties with pulse pressure, we could not consider such situations.

Finally, as mentioned earlier, an off-line strain calculation was required on ST-IVUS analysis, which is too time-consuming for routine clinical use. However, many commercial vendors already have individual speckle-tracking techniques. Therefore, real-time ST-IVUS may be developed in the future to overcome this obstacle.

Declarations

References

1. Kato T, Noda T, Tanaka S, Yagasaki H, Iwama M, Tanihata S, Arai M, Minatoguchi S, Okura H (2022) Impact of accelerated washout of Technetium-99m-sestamibi on exercise tolerance in patients with acute coronary syndrome: single-center experience. Heart Vessels. https://doi.org/10.1007/s00380-022-02058-3

2. Amano H, Noike R, Yabe T, Watanabe I, Okubo R, Koizumi M, Toda M, Ikeda T (2020) Frailty and coronary plaque characteristics on optical coherence tomography. Heart Vessels 35:750–761

3. Bentzon JF, Otsuka F, Virmani R, Falk E (2014) Mechanisms of plaque formation and rupture. Circ Res 114:1852–1866

4. Sano K, Kawasaki M, Ishihara Y, Okubo M, Tsuchiya K, Nishigaki K, Zhou X, Minatoguchi S, Fujita H, Fujiwara H (2006) Assessment of vulnerable plaques causing acute coronary syndrome using integrated backscatter intravascular ultrasound. J Am Coll Cardiol 47:734–741

5. Nishida T, Hiro T, Takayama T, Sudo M, Haruta H, Fukamachi D, Hirayama A, Okumura Y (2021) Clinical significance of microvessels detected by in vivo optical coherence tomography within human atherosclerotic coronary arterial intima: a study with multimodality intravascular imagings. Heart Vessels 36:756–765

6. Murata N, Hiro T, Takayama T, Migita S, Morikawa T, Tamaki T, Mineki T, Kojima K, Akutsu N, Sudo M, Kitano D, Fukamachi D, Hirayama A, Okumura Y (2019) High shear stress on the coronary arterial wall is related to computed tomography-derived high-risk plaque: a three-dimensional computed tomography and color-coded tissue-characterizing intravascular ultrasonography study. Heart Vessels 34:1429–1439

7. Sato H, Kawasaki M, Morita N, Fujiwara H, Minatoguchi S (2015) Distribution of tissue characteristics of coronary plaques evaluated by integrated backscatter intravascular ultrasound: Differences between the inner and outer vessel curvature. J Cardiol 66:489–495

8. Okubo M, Kawasaki M, Ishihara Y, Takeyama U, Yasuda S, Kubota T, Tanaka S, Yamaki T, Ojio S, Nishigaki K, Takemura G, Saio M, Takami T, Fujiwara H, Minatoguchi S (2008) Tissue characterization of coronary plaques: comparison of integrated backscatter intravascular ultrasound with virtual histology intravascular ultrasound. Circ J 72:1631–1639

9. Okubo M, Kawasaki M, Ishihara Y, Takeyama U, Kubota T, Yamaki T, Ojio S, Nishigaki K, Takemura G, Saio M, Takami T, Minatoguchi S, Fujiwara H (2008) Development of integrated backscatter intravascular ultrasound for tissue characterization of coronary plaques. Ultrasound Med Biol 34:655–663

10. Kawasaki M, Hattori A, Ishihara Y, Okubo M, Nishigaki K, Takemura G, Saio M, Takami T, Minatoguchi S (2010) Tissue characterization of coronary plaques and assessment of thickness of fibrous cap using integrated backscatter intravascular ultrasound. Comparison with histology and optical coherence tomography. Circ J 74:2641–2648

11. Ohota M, Kawasaki M, Ismail TF, Hattori K, Serruys PW, Ozaki Y (2012) A histological and clinical comparison of new and conventional integrated backscatter intravascular ultrasound (IB-IVUS). Circ J 76:1678–1686

12. Ishihara Y, Kawasaki M, Hattori A, Imai H, Takahashi S, Sato H, Kubota T, Okubo M, Ojio S, Nishigaki K, Takemura G, Fujiwara H, Minatoguchi S (2012) Relationship among coronary plaque compliance, coronary risk factors and tissue characteristics evaluated by integrated backscatter intravascular ultrasound. Cardiovasc Ultrasound 10:32

13. Kawasaki M, Tanaka R, Tanaka S, Minatogchi S, Yoshida A, Naruse G, Watanabe T, Tanaka T, Ono K, Kanamori A, Noda T (2018) Speckle-tracking on left atrium and coronary artery. J. JCS Cardiol. 27:43–48

14. Tanaka S, Kawasaki M, Noda T, Segawa T, Tsugita N, Fuseya T, Iwama M, Yagasaki H, Kawaguchi T, Kato T, Watanabe S, Minagawa T, Minatoguchi S, Okura H (2022) Observation of plaque behavior and tissue characterization of coronary plaque using speckle tracking intravascular ultrasound (ST-IVUS) and iMap imaging system. Heart Vessels. https://doi.org/10.1007/s00380-022-02056-5

15. Rodriguez-Granillo GA, García-García HM, Valgimigli M, Schaar JA, Pawar R, van der Giessen WJ, Regar E, van der Steen AF, de Feyter PJ, Serruys PW (2006) In vivo relationship between compositional and mechanical imaging of coronary arteries. Insights from intravascular ultrasound radiofrequency data analysis. Am Heart J 15:1025.e1–6

16. Brugaletta S, Garcia-Garcia HM, Serruys PW, Maehara A, Farooq V, Mintz GS, de Bruyne B, Marso SP, Verheye S, Dudek D, Hamm CW, Farhat N, Schiele F, McPherson J, Lerman A, Moreno PR, Wennerblom B, Fahy M, Templin B, Morel MA, van Es GA, Stone GW (2012) Relationship between palpography and virtual histology in patients with acute coronary syndromes. JACC Cardiovasc Imaging 5:S19-27

17. De Bruyne B, Hersbach F, Pijls NH, Bartunek J, Bech JW, Heyndrickx GR, Gould KL, Wijns W (2001) Abnormal epicardial coronary resistance in patients with diffuse atherosclerosis but "Normal" coronary angiography. Circulation 104:2401–2406

18. Loree HM, Kamm RD, Stringfellow RG, Lee RT (1992) Effects of fibrous cap thickness on peak circumferential stress in model atherosclerotic vessels. Circ Res 71:850–858

19. Gijsen FJ, Wentzel JJ, Thury A, Mastik F, Schaar JA, Schuurbiers JC, Slager CJ, van der Giessen WJ, de Feyter PJ, van der Steen AF, Serruys PW (2008) Strain distribution over plaques in human coronary arteries relates to shear stress. Am J Physiol Heart Circ Physiol 295:H1608-1614

20. Oishi Y, Miyoshi H, Mizuguchi Y, Iuchi A, Nagase N, Oki T (2011) Aortic stiffness is strikingly increased with age ≥ 50 years in clinically normal individuals and preclinical patients with cardiovascular risk factors: assessment by the new technique of 2D strain echocardiography. J Cardiol 57:354–359

21. Hansen HH, de Borst GJ, Bots ML, Moll FL, Pasterkamp G, de Korte CL (2016) Validation of noninvasive in vivo compound ultrasound strain imaging using histologic plaque vulnerability features. Stroke 47:2770–2775

22. Keymel S, Heinen Y, Balzer J, Rassaf T, Kelm M, Lauer T, Heiss C (2011) Characterization of macro-and microvascular function and structure in patients with type 2 diabetes mellitus. Am J Cardiovasc Dis 1:68–75

23. Chatterjee S, Fujiwara K, Pérez NG, Ushio-Fukai M, Fisher AB (2015) Mechanosignaling in the vasculature: emerging concepts in sensing, transduction and physiological responses. Am J Physiol Heart Circ Physiol 308:H1451-1462

24. Chistiakov DA, Orekhov AN, Bobryshev YV (2015) Endothelial barrier and its abnormalities in cardiovascular disease. Front Physiol 6:365

25. Podgórski M, Grzelak P, Szymczyk K, Szymczyk E, Drożdż J, Stefańczyk L (2015) Peripheral vascular stiffness, assessed with two-dimensional speckle tracking versus the degree of coronary artery calcification, evaluated by tomographic coronary artery calcification index. Arch Med Sci 11:122–129

26. Lavi S, Bae JH, Rihal CS, Prasad A, Barsness GW, Lennon RJ, Holmes DR Jr, Lerman A (2009) Segmental coronary endothelial dysfunction in patients with minimal atherosclerosis is associated with necrotic core plaques. Heart 95:1525–1530

27. Choi BJ, Prasad A, Gulati R, Best PJ, Lennon RJ, Barsness GW, Lerman LO, Lerman A (2013) Coronary endothelial dysfunction in patients with early coronary artery disease is associated with the increase in intravascular lipid core plaque. Eur Heart J 34:2047–2054

28. Choi BJ, Matsuo Y, Aoki T, Kwon TG, Prasad A, Gulati R, Lennon RJ, Lerman LO, Lerman A (2014) Coronary endothelial dysfunction is associated with inflammation and vasa vasorum proliferation in patients with early atherosclerosis. Arterioscler Thromb Vasc Biol 34:2473–2477

29. de Korte CL, Sierevogel MJ, Mastik F, Strijder C, Schaar JA, Velema E, Pasterkamp G, Serruys PW, van der Steen AF (2002)

Identification of atherosclerotic plaque components with intravascular ultrasound elastography in vivo: a Yucatan pig study. Circulation 105:1627–1630

30. Schaar JA, De Korte CL, Mastik F, Strijder C, Pasterkamp G, Boersma E, Serruys PW, Van Der Steen AF (2003) Characterizing vulnerable plaque features with intravascular elastography. Circulation 108:2636–2641

31. Gorcsan J 3rd, Tanaka H (2011) Echocardiographic assessment of myocardial strain. J Am Coll Cardiol 58:1401–1413

32. Beaussier H, Naggara O, Calvet D, Joannides R, Guegan-Massardier E, Gerardin E, Iacob M, Laloux B, Bozec E, Bellien J, Touze E, Masson I, Thuillez C, Oppenheim C, Boutouyrie P, Laurent S (2011) Mechanical and structural characteristics of carotid plaques by combined analysis with echotracking system and MR imaging. JACC Cardiovasc Imaging 4:468–477

33. Lopata RG, Nillesen MM, Hansen HH, Gerrits IH, Thijssen JM, de Korte CL (2009) Performance evaluation of methods for two-dimensional displacement and strain estimation using ultrasound radio frequency data. Ultrasound Med Biol 35:796–812

34. Tanaka S, Noda T, Kawasaki M, Segawa T, Tsugita N, Fuseya T, Kubota T, Iwama M, Nishigaki K, Watanabe S, Minagawa T, Ohashi H, Minatoguchi S (2019) Relationship between electrical conduction and phasic left atrial function: P-wave signal-averaged electrocardiography and time-left atrial volume curve assessments using two-dimensional speckle-tracking echocardiography. Heart Vessels 34:1212–1220

35. Tanaka S, Segawa T, Noda T, Tsugita N, Fuseya T, Kawaguchi T, Iwama M, Watanabe S, Minagawa T, Minatoguchi S, Okura H (2021) Assessment of visit-to-visit variability in systolic blood pressure over 5 years and phasic left atrial function by two-dimensional speckle-tracking echocardiography. Heart Vessels 36:827–835

36. Pirat B, Khoury DS, Hartley CJ, Tiller L, Rao L, Schulz DG, Nagueh SF, Zoghbi WA (2008) A novel feature-tracking echocardiographic method for the quantitation of regional myocardial function: validation in an animal model of ischemia-reperfusion. J Am Coll Cardiol 51:651–659

37. Amzulescu MS, De Craene M, Langet H, Pasquet A, Vancraeynest D, Pouleur AC, Vanoverschelde JL, Gerber BL (2019) Myocardial strain imaging: review of general principles, validation, and sources of discrepancies. Eur Heart J Cardiovasc Imaging 20:605–619

Authors and Affiliations

Shinichiro Tanaka[1] · **Masanori Kawasaki**[2] · **Toshiyuki Noda**[3] · **Tomonori Segawa**[1] · **Makoto Iwama**[3] · **Hiroto Yagasaki**[3] · **Takahiro Ueno**[3] · **Takashi Yoshizane**[3] · **Takashi Kato**[3] · **Takahiro Fuseya**[1] · **Sachiro Watanabe**[3] · **Taro Minagawa**[4] · **Shinya Minatoguchi**[5] · **Hiroyuki Okura**[6]

[1] The Department of Cardiology, Asahi University Hospital, 3-23 Hashimoto-cho, Gifu 500-8523, Japan

[2] Gifu Heart Center, Gifu, Japan

[3] Gifu Prefectural General Medical Center, Gifu, Japan

[4] Gifu Cardiovascular Institution, Gifu, Japan

[5] Gifu Municipal Hospital, Gifu, Japan

[6] Second Department of Internal Medicine, Gifu University Graduate School of Medicine, Gifu, Japan